Cement and Concrete Research 40 (2010) 284–292

Contents lists available at ScienceDirect

Cement and Concrete Research

journal homepage: http://ees.elsevier.com/CEMCON/default.asp

Carbonation of CH and C–S–H in composite cement pastes containing high amounts of BFS

Paulo H.R. Borges [a,*], Juliana O. Costa [b], Neil B. Milestone [a], Cyril J. Lynsdale [b], Roger E. Streatfield [c]

[a] Immobilisation Science Laboratory, Department of Engineering Materials, University of Sheffield, Mappin Street, Sheffield, S1 3JD, UK
[b] Department of Civil and Structural Engineering, University of Sheffield, Mappin St., Sheffield S1 3JD, UK
[c] Magnox South, C11 (upper), Berkeley Centre, Berkeley, Glos. GL13 9PB, UK

ARTICLE INFO

Article history:
Received 31 July 2008
Accepted 29 October 2009

Keywords:
B. Calcium–silicate–hydrate (C–S–H)
B. Thermal analysis
C. Carbonation
D. Granulated blast-furnace slag

ABSTRACT

3:1 BFS:OPC, 9:1 BFS:OPC and 9:1 alkali activated BFS:OPC pastes cured at 20 °C and 60 °C for 90 days were submitted to accelerated carbonation under 5% CO_2, 60% relative humidity and 25 ± 5 °C for 21 days. TGA/DTG was used to quantify the amounts of carbonates formed from calcium hydroxide (CH) and calcium silicate hydrate (C–S–H), based on the CH and carbonate contents before and after carbonation. Apparent dry density, apparent porosity and gas permeability were measured before and after accelerated carbonation testing, and the phenolphthalein method used to determine the accelerated carbonation rate. The results showed that samples cured at elevated temperature, i.e. 60 °C, were initially less porous and, therefore, had decreased levels of both total carbonation and C–S–H carbonation. In addition, the carbonation of C–S–H was significantly higher in pastes that contained less CH before carbonation. In the activated 9:1 BFS:OPC, the carbonation of C–S–H was extensive, despite a lower carbonation rate than the analogous non-activated system. In the particular case of activated 9:1 BFS:OPC, a shift in the DTG decarbonation pattern was observed and XRD showed that aragonite was present as one of the calcium carbonate polymorphs.

1. Introduction

Blended cements containing large replacements of ordinary Portland cement (OPC) with blast-furnace slag (BFS) are currently used for encapsulation of nuclear waste in the UK. Up to 90% BFS is employed in encapsulation pastes [1], amounts which are much higher than those used in the construction industry. These percentages were defined to help reduce the heat evolution of the mixes and avoid problems associated with thermal cracking and loss of durability, and to ensure the rheology of the pastes is sufficiently fluid for mixing and pouring into the encapsulation drums. Previous research has shown that the hydration in these systems is limited. Hill and Sharp [2] showed that the hydration of the BFS in a 9:1 BFS:OPC paste (90% OPC replacement) did not progress far; Utton [3] used SEM image analysis to quantify the hydration of the BFS/OPC systems and concluded that the amount of reacted slag in the 9:1 system was approximately 45% after 2 years of hydration at 20 °C but increased to 55% when cured at 60 °C. In the 4:1 system, slag hydration was 65% at 20 °C. Gorce and Milestone [4] following the changes in water phases by ^{1}H NMR relaxometry, showed further evidence that the hydration of 9:1 BFS:OPC paste was limited, with little change after approximately 28 days.

As these replacement levels are not commonly studied, there is little information in the literature on the durability of these systems and how chemical attack, e.g. carbonation, may affect the microstructure and physical properties.

1.1. Carbonation of CH and C–S–H

Carbonation is a common type of attack in cement paste and concretes. The process begins when CO_2 penetrates into the cement matrix, dissolving in the pore solution to produce HCO_3^- and CO_3^{2-} ions, which react with Ca^{2+} from calcium hydroxide (CH), calcium silicate hydrate (C–S–H) and the hydrated calcium aluminates and ferro-aluminates to precipitate as various forms of calcium carbonate ($CaCO_3$), silica gel and hydrated aluminium and iron oxides [5]. Generally, an initial reduction of porosity is expected because CH is the first phase attacked and the volume of the carbonates (calcite) formed is 11–12% greater than the volume of CH. Therefore, it is frequent to find an increase in the weight of carbonated samples, as well as lower porosity and higher compressive strength at early ages of carbonation [6,7]. This is the case for low porosity OPC pastes, where calcite formation decreases the overall porosity, preventing further diffusion of CO_2 and reducing the carbonation attack. However, when the porosity in pastes is sufficiently high to permit constant CO_2 diffusion, the CH is further depleted and the interlayer calcium from C–S–H also reacts with carbon dioxide [8]. The removal of interlayer Ca^{2+} ions creates an excess of negative charges, which are balanced through subsequent formation of

* Corresponding author. Civil Engineering Department, Federal Centre for Technological Education of Minas Gerais (CEFET-MG), Av. Amazonas 7565, Belo Horizonte, M.G., Brazil.
E-mail address: pborges@civil.cefetmg.br (P.H.R. Borges).

0008-8846/$ – see front matter © 2009 Elsevier Ltd. All rights reserved.
doi:10.1016/j.cemconres.2009.10.020

Si–OH groups. Condensation of neighbouring Si–OH groups to Si–O–Si linkages then forms silica gel [9]. This condensation increases the mean silicate chain length and forms bridges between neighbouring regions, thus pulling them closer together leading to shrinkage. As a result, CO_2 attack causes polymerisation of the silicate chains in C–S–H, which may cause a volumetric decrease (shrinkage) and cracking, coarsening the porosity. Non-carbonated pastes are usually characterized by pores in the range of $10<r<50$ nm, whereas silica gel has large pores, with $100<r<1000$ nm [10].

There is evidence in the literature [11] that CO_2 simultaneously reacts with C–S–H and CH and that the decalcification of C–S–H takes place prior to the formation of silica gel, the latter starting at later stages of carbonation. CH carbonation may be initially more rapid than that of the C–S–H gel, but this situation soon reverses because of the formation of a layer of $CaCO_3$ micro crystals at the surface of CH [11,12]. In blended cement pastes, where the amount of CH is reduced due to pozzolanic reaction, carbonation of C–S–H seems to be even more dependent on the permeability of the pastes. Rapid decalcification of C–S–H is expected in highly permeable pastes, accompanied by carbonation shrinkage, which is accelerated when the $CaO:SiO_2$ molar ratio (C/S) is reduced below 1.2 [9]. On the other hand, carbonation of the low C/S ratio C–S–H might not be a risk when the blended pastes have low permeability to hinder the CO_2 ingress.

Over the years, different techniques have been used to study the effect of carbonation on cement pastes [13–21]. In the 60s, Cole and Kroone [13] used DTA, TGA and XRD to study how calcium carbonate was held in mortars and C–S–H pastes exposed to different conditions. The greater part of the carbon dioxide taken up by mortar and C–S–H pastes was not held as calcite, which is the main stable calcium carbonate polymorph, but rather as a poorly crystallized and amorphous calcium carbonate, as well as the crystalline forms of vaterite and aragonite which decompose at lower temperatures than calcite. Cole and Kroone concluded that the formation of vaterite or aragonite could represent different stages of carbonation or merely different pH conditions, as high pH seemed to favor the formation of vaterite over aragonite. Slegers and Rouxhet [14] used XRD and infrared spectroscopy (IR) to assess the carbonation products in pastes of hydrated C_3S. The latter method is believed to be more accurate for the identification of the partial carbonation front rather than the well-known phenolphthalein method [15] and clearly identifies silica gel. In that work [14], calcite was not formed and the authors suggested that the formation of aragonite was associated with carbonation of young pastes, where hydration was limited.

A recent study using Raman spectroscopy in combination with XRD [16] has associated the type of calcium carbonate polymorph with the C/S ratio of C–S–H in carbonated pastes: vaterite was found when C–S–H had $C/S \geq 0.67$ whereas aragonite was present when $C/S \leq 0.50$. This is in agreement with previous work of Nishikawa and Suzuki [17] and Groves et al. [11]. The first authors observed the formation of vaterite as single $CaCO_3$ polymorph when carbonation reduced the C/S ratio in concretes from 1.5 to 1.0 whereas Groves et al. [11] identified only vaterite and calcite as the crystalline $CaCO_3$ polymorphs, when the C/S ratio was still slightly higher than 1.0. Thierry et al. [12] did not report the C/S for the C–S–H in the carbonated pastes they studied, but observed that CO_2 was held in stable, metastable and amorphous forms of $CaCO_3$ and that the thermal stability of $CaCO_3$ was lower as the carbonation of C–S–H increased. In general, there is an agreement that the extent of carbonation of C–S–H is a function of the C/S ratio, i.e. pastes with different C/S ratio have distinct C–S–H anion polymerisation [18] and that low C/S ratio C–S–H forms more silica gel when CH is not present as a buffer phase [19].

Regarding the performance of blended pastes under carbonation attack, most of research has been limited to the effect of carbonation on the physical properties with little study on the effects of carbonation of the main phases [22–26]. As C–S–H has a low C/S ratio for blended pastes, it is expected that the carbonation mechanisms in blended pastes will be different from that of neat OPC or C–S–H pastes [10,27].

In addition, there is likely to be an optimum percentage of supplementary pozzolanic materials used in encapsulation mixes, which either ensures that porosity and permeability are low to prevent CO_2 diffusion or guarantees that there is sufficient CH in the system to buffer C–S–H decomposition.

The aim of this paper is to determine (i) the extent of carbonation of CH and C–S–H in blended cement pastes containing high amounts of BFS, which are known to have a low degree of hydration [2–4]; (ii) the effect of curing temperature (20 °C and 60 °C) on the carbonation rate and carbonation of the main phases, CH and C–S–H; (iii) the changes in apparent density, porosity and permeability after the different encapsulation mixes are subjected to carbonation. If the C–S–H in the composite blends used for encapsulation, which contain either 75% or 90% BFS, is severely attacked by CO_2, then durability may be reduced, as the microstructure will be changed, opening the matrix to the possible release of radionuclides by leaching. Therefore, it is important to determine which phases are attacked during the carbonation process for the mixes currently employed. If only CH is carbonated, the overall porosity may be decreased; however, if C–S–H is the main phase attacked, the porosity and permeability may be increased considerably.

2. Experimental

OPC and BFS were produced by Castle Cement and Scunthorpe, respectively, and supplied by British Nuclear Fuels Ltd (BNFL). Their compositions are shown in Table 1. The elemental composition of ordinary Portland cement (OPC), and BFS was conducted by XRF. The loss on ignition (LOI) was obtained by the method described in the British Standard BS EN 196-1. While the OPC has comparable fineness to that used in construction, the BFS is very coarse with a Blaine fineness of only 260 m^2/kg.

The formulations used in this work are described in Table 2. Pastes 9S1C and 3S1C contain 90% and 75% of BFS, respectively, which are the upper and lower limits of the formulation envelope used for BFS/OPC encapsulation pastes. The water to solids ratio currently employed in BFS/OPC blends is 0.33. The third formulation, 9S1CA, is a modification of the 9S1C but activated with a sodium silicate solution (Na_2SiO_3) to promote the reactivity of BFS in a 9:1 system and overcome the limited hydration pointed out in the literature [2–4]. The activator contained 6.1 wt.% Na_2O, 7.5 wt.% SiO_2 and 86.4 wt.% H_2O.

Two to three kilograms of paste were mixed in a Hobart mixer for 30 min. Water was always added first and the powder afterwards. For 9S1CA, the solution containing Na_2SiO_3 and NaOH was added to the mixing water to give a total water to solids ratio of 0.33. The fresh pastes were moulded in cylinders of 22 mm diameter × 45 mm height. Sedimentation of the samples was avoided by tumbling the samples on a roller mixer for the first 24 h. After that, samples were cured under water at 20 °C and 60 °C for 90 days, to assess the effect of the curing temperature on the durability to carbonation. The suffixes 20 and 60 are used with the sample name to differentiate the samples cured at these two temperatures, e.g. 3S1C-20, 3S1C-60.

2.1. Thermogravimetric analysis (TGA)

One cylinder of each formulation was broken with a hammer at 90 days and small pieces were quenched in acetone for 7 days to stop

Table 1
Elemental composition of the materials used.

	SiO_2	Al_2O_3	Fe_2O_3	CaO	MgO	K_2O	Na_2O	TiO_2	SO_3	LOI
OPC	20.96	5.24	2.61	64.58	2.09	0.59	0.28	–	2.46	0.73
BFS	34.50	13.74	0.97	42.10	7.29	0.49	0.22	–	–	−1.05

Table 2
Formulation of pastes for assessment of durability.

Sample name	Formulation	Composition	w/s[a]	Notes
3S1C	3:1 BFS:OPC	75% BFS/25%OPC	0.33	Ends of formulation envelope used for encapsulation pastes
9S1C	9:1 BFS:OPC	90% BFS/10%OPC	0.33	
9S1CA	9:1 BFS:OPC (activated)	90% BFS/10%OPC + Na_2SiO_3	0.33	Altered formulation, containing sodium silicate as external activator of BFS

[a] w/s corresponds to water to solids ratio. The solids were (OPC + BFS) and (OPC + BFS + solids in activator, for 9S1CA).

the hydration. They were subsequently kept in a desiccator under vacuum to dry out and to avoid carbonation. These samples were then ground using a pestle and mortar, sieved and particles smaller than 63 μm were used for TGA, performed in a Perkin Elmer Pyris 1 instrument, heating from 30 °C to 1000 °C at 10 °C per minute under a nitrogen atmosphere. The weight loss from TGA and the first derivative (DTG) were used to estimate the amounts of calcium hydroxide (CH) and calcium carbonate (CC) present in each sample.

It is known that OPC and BFS may contain some carbonates. TGA of the raw materials showed that the amounts of carbonates were negligible. It was assumed, therefore, that all carbonates identified in the pastes by TGA originated from calcium hydroxide. The CO_2 loss in the decarbonation region (600–750 °C) (dc_{loss}) was converted into a calcium hydroxide loss ($CH_{dc\text{-}loss}$) and added to the calcium hydroxide ($CH_{dh\text{-}loss}$) calculated from the dehydroxylation region (400–500 °C) (dh_{loss}) to give a total calcium hydroxide initially available (CH_{total}). The amount of calcium hydroxide from the decarbonation loss ($CH_{dc\text{-}loss}$) was calculated using Eqs. (1)–(3) (losses are calculated based on % loss basis).

$$\underset{74\,g/mol}{Ca(OH)_2} + \underset{44\,g/mol}{CO_2} \rightarrow \underset{100\,g/mol}{CaCO_3} + \underset{18\,g/mol}{H_2O} \quad (1)$$

$$\%CC = \frac{dc_{loss} \cdot 100}{44} = 2.27 \cdot dc_{loss} \quad (2)$$

$$\%CH_{dc-loss} = \frac{\%CC \cdot 74}{100} = \frac{2.27 \cdot dc_{loss} \cdot 74}{100} = 1.68 \cdot dc_{loss} \quad (3)$$

The calcium hydroxide content from the TGA dehydroxylation loss was calculated using Eqs. (4) and (5).

$$\underset{74\,g/mol}{Ca(OH)_2} \rightarrow \underset{56\,g/mol}{CaO} + \underset{18\,g/mol}{H_2O} \quad (4)$$

$$\%CH_{dh-loss} = \frac{dh_{loss} \cdot 74}{18} = 4.11 \cdot dh_{loss} \quad (5)$$

The total amount of calcium hydroxide (CH_{total}) was calculated by adding the results from Eqs. (3) and (5), as shown in Eq. (6).

$$\%CH_{total} = \%CH_{dc-loss} + \%CH_{dh-loss} = 1.68 \cdot dc_{loss} + 4.11 \cdot dh_{loss} \quad (6)$$

2.2. Carbonation of CH and C–S–H

The extent of carbonation of CH and C–S–H was estimated from the amounts of calcium hydroxide and carbonates before and after carbonation, determined by TGA. The percentage of carbonates formed by carbonation of C–S–H was estimated by subtracting the percentages found, as explained in Table 3. The columns in this table are divided into "Before carbonation" and "After carbonation". They are also labelled from "A" to "H", where columns A, B and C are data before carbonation and D to H data after accelerated carbonation. Columns A, B, D and E are the amounts of CH and CC before and after accelerated carbonation, calculated using the dehydroxylation and decarbonation losses from TGA/DTG and the Eqs. (2) and (5) in Section 2.1. The initial amount of CH in the pastes is expressed in column C, using Eq. (6). Alternatively, the initial amount of CH may be directly calculated from columns A and B, as in Eq. (7).

$$\%CH_{initial} = \%CH + \frac{\%CC \cdot 74\,g/mol}{100\,g/mol} = \%CH + 0.74\%CC = (A) + 0.74 \cdot (B) \quad (7)$$

Column F estimates the percentage of initial CH that had carbonated, i.e., subtracting the %CH after carbonation (D) from %CH before accelerated testing (C). Column G calculates the corresponding amount of CC from the total CH that carbonated (F), as shown in Eq. (8).

$$\%CC = \frac{\%CH \cdot 100}{74} = 1.35 \cdot \%CH = 1.35 \cdot (F) \quad (8)$$

Once the %CC from calcium hydroxide has been estimated, then the %CC arising from C–S–H may be calculated. It is equal to the total amount of carbonates present after accelerated carbonation (E) minus the carbonates formed from calcium hydroxide (G).

This method is not completely accurate, as it is based on several assumptions: (a) the onset temperatures on TGA/DTG were visually determined and, therefore, represent a source of error; (b) only one sample of each paste formulation was characterised by TGA/DTG and the errors in the results were not calculated; (c) the method assumes that all of the initial carbonates were products of the carbonation of CH; Hence, it does not take into account any carbonates formed by reaction of C–S–H with CO_2 before accelerated carbonation (d) it was assumed that CO_2 is the only gas emitted in the temperature range 550–700 °C.

Note that some initial carbonation of samples (before accelerated testing) was due to atmospheric exposure during sample preparation (grinding with a pestle and mortar), as this was not carried out in a CO_2-free environment.

2.3. Accelerated carbonation

Cylinders of each mix were submitted to accelerated carbonation after 90 days of curing at the respective temperatures. Neat OPC paste cylinders (w/c = 0.33) cured at 20 °C and 60 °C for 90 days and used for comparison. They are referred to as PC-20 and PC-60, respectively, hereafter. The carbonation test was carried out in a controlled tank using 5% CO_2, 60% relative humidity and 25 ± 5 °C. Samples were taken from the curing regime, allowed to dry out in the lab (50–60% humidity) for 48 h and then submitted to accelerated carbonation testing. Oven drying was not carried out as pre-treatment to accelerated carbonation to avoid microcracking in the samples. From 1 to 21 days the test samples were broken and a phenolphthalein solution of 1 g phenolphthalein dissolved in 30 g ethanol and 70 g distilled water was sprayed onto the freshly broken surfaces to measure the depth of carbonation at the specific age. The depth of carbonation reported is the average of five measurements. The testing was stopped at 21 days because by then some samples were completely carbonated and not coloured by phenolphthalein so this test could not assess the carbonation rate anymore.

Eq. (9) describes the carbonation rate, where X is the depth of carbonation, t is the time during which carbonation has taken place, C is the carbonation rate and X_0 is the initial carbonation, usually small or zero [5]. Assuming that X_0 is nil or negligible, Eq. (9) can be simplified to Eq. (10).

$$X = X_0 + C \cdot \sqrt{t} \quad (9)$$

Table 3
TGA data before and after carbonation of 90 days BFS/OPC pastes and an estimation of the extent of carbonation of C–S–H.

Grouts after 7 and 21 days of accelerated carbonation	Before carbonation (90 days of hydration)			After carbonation				
	% CH from TGA	% CC from TGA	Calculation of initial % CH	% CH from TGA	% CC from TGA	Amount of CH that carbonated	Expected % of CC from carbonating CH	Carbonates formed by C–S–H
	(A)	(B)	(C) = (A) + 0.74 × (B)	(D)	(E)	(F) = (C) = (D)	(G) = 1.35 × (F)	(H) = (E) − (G)
3S1C-20 (after7 days)	4.9	2.4	6.6	4.2	3.5	2.4	3.2	0.3
3S1C-20 (after 21 days)	4.9	2.4	6.6	2.7	7.0	3.9	5.3	1.7
3S1C-60 (after7 days)	5.4	2.4	7.2	5.0	3.1	2.2	3.0	0.1
3S1C-60 (after 21 days)	5.4	2.4	7.2	3.5	6.7	3.7	5.0	1.7
9S1C-20 (after7 days)	2.7	1.7	3.9	0.0	7.0	3.9	5.3	1.6
9S1C-20 (after 21 days)	2.7	1.7	3.9	0.0	11.5	3.9	5.3	6.1
9S1C-60 (after7 days)	2.5	1.8	3.9	0.0	8.3	3.9	5.2	3.1
9S1C-60 (after 21 days)	2.5	1.8	3.9	0.0	10.6	3.9	5.2	5.4
9S1CA-20 (after7 days)	0.0	1.2	0.9	0.0	8.9	0.9	1.2	7.7
9S1CA-20 (after 21 days)	0.0	1.2	0.9	0.0	13.5	0.9	1.2	12.3
9S1CA-60 (after7 days)	0.0	0.9	0.6	0.0	8.4	0.6	0.9	7.6
9S1CA-60 (after 21 days)	0.0	0.9	0.6	0.0	9.8	0.6	0.9	8.9

$$X = C \cdot \sqrt{t} \tag{10}$$

The cylinders were broken after 7 days and 21 days of accelerated carbonation and samples for XRD and TGA were obtained by drilling one or more holes at approximately 2 mm from the surface of the samples (Fig. 1), in the discoloured region of the phenolphthalein sprayed sample. XRD was performed from $2\theta = 20°$ to 60° at 0.5° per minute using a step size of 0.01°, in order to clearly differentiate the peaks of aragonite, vaterite and calcite. TGA after carbonation was used to determine the amount of calcium hydroxide and total amount of carbonates, as in Eqs. (2) and (5).

The samples from paste PC-20 and PC-60 (neat OPC pastes) were not characterised by TGA. The carbonation shown by these pastes was very limited, as no discernable carbonation layer was shown by the phenolphthalein test over the 21 days of accelerated testing. The structure was probably so dense due to the high degree of hydration and low water to cement ratio (0.33), that the early formation of calcium carbonate on the surface of the material closed the surface pores and stopped the carbonation. No further carbonation (detected by the phenolphthalein method) took place.

2.4. Apparent density and porosity

The apparent dry density was determined by dividing the oven-dried (50 °C overnight) mass of the cylindrical samples by their volume. The volume was calculated from the dimensions of the samples, which were measured with a calliper. The same samples used for apparent density were also used for apparent porosity, determined by water absorption under vacuum whereby apparent porosity is expressed as the percentage of the volume of absorbed water in the bulk volume of specimen. Three samples were used and the average and standard deviation determined. Apparent dry density and porosity were measured before carbonation and after 21 days of accelerated testing.

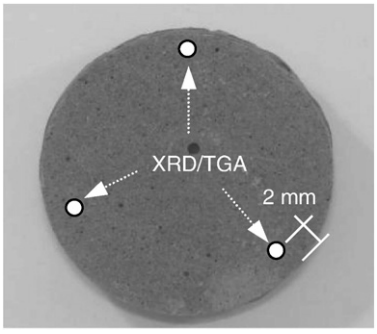

Fig. 1. Extraction of the samples for XRD/TGA.

2.5. Gas permeability

Oxygen permeability was carried out using the Leeds permeameter described by Cabrera and Lynsdale [28]. In this method, pressurised oxygen is forced to flow vertically through a sample, which is laterally sealed by a rubber cylinder inside a steel cylinder. The gas flow rate is measured using a bubble flow meter and is recorded after a steady state of flow has been reached (approximately 30 min from the start of the experiment). The intrinsic permeability may be calculated by the Eq. (11) [28,29], where k is the intrinsic permeability (m^2); L is the length of the specimen (m); A is the cross-sectional area of specimen (m^2); Q is the flow rate (cm^3/s); P_1 is the absolute applied pressure (bar), P_2 is the pressure at which the flow rate is measured, equal to 1 bar. The constant 2.02×10^{-16} accounts for the transformation of units.

$$k = \frac{2 \cdot (2.02 \cdot 10^{-16}) \cdot Q \cdot P_2 \cdot L}{A \cdot (P_1^2 - P_2^2)} \tag{11}$$

Four cylindrical samples of 22 × 45 mm were used for assessing the intrinsic permeability of the pastes before and after 21 days of carbonation. The results are expressed in terms of the mean and the standard deviation.

3. Results and discussion

3.1. Carbonation rate (phenolphthalein method)

Fig. 2 shows the carbonation rate for the BFS:OPC pastes studied. As mentioned above, PC pastes did not show any carbonation that could be measured by the phenolphthalein method. It is important to note that the carbonation rate increased with the increasing amount of BFS in the mixes; the BFS used is very coarse (Blaine 260 m^2/kg) and did not react very much with time [2–4].

The consequence is that 9S1C (90% BFS) carbonated significantly faster than 3S1C (75% BFS). Curing at 60 °C decreased the carbonation in all BFS-OPC pastes. The activation of 9:1 BFS:OPC appeared to be effective only when 60 °C curing was performed, as the carbonation rate in 9S1CA-20 was the highest among the BFS/OPC pastes.

3.2. Changes in apparent density and porosity

Fig. 3 shows the apparent dry density of the pastes before and after carbonation. The density increased for all pastes due to CO_2 uptake, except for the neat OPC pastes. In fact, PC-20 pastes showed little increase in density after carbonation, with PC-60 showing no increase at all. These results are in line with the phenolphthalein method, which showed no carbonation occurred for the PC pastes. Fig. 3 also indicates that the increase in density after carbonation is proportional to the amount of BFS for the remaining BFS:OPC pastes.

Table 4 tabulates the results of Fig. 3 and shows that the CO_2 uptake is higher for samples cured at lower temperature. So, high curing temperature had a positive effect on the microstructure given that (i) the CO_2 uptake has been reduced; (ii) the carbonation rate has slowed down; and (iii) less carbonates form with a consequent lower increase in density after carbonation.

Fig. 4 shows the apparent porosity before and after carbonation. The apparent porosity at 90 days (before carbonation) increased in the pastes as the BFS content increased. Porosity results are in line with apparent density the carbonation rates for BFS:OPC pastes. As in many other studies, the porosity decreased with the formation of calcium carbonate in the structure [5–7]. The pastes that carbonated the most, i.e. 9S1C and 9S1CA, increased in density and the reduction in porosity after carbonation appeared slightly higher.

3.3. Changes in oxygen permeability

Isolated results in Section 3.2 may give an impression that carbonation is not an issue for encapsulation pastes, as samples increased in density and had lower overall porosity after accelerated testing. However, these tests showed up an important issue: the samples cracked during carbonation. Fig. 5 shows pastes 9S1CA-20 and 9S1CA-60 after only 7 days of accelerated carbonation. The lighter rings in those samples do not correspond to a carbonation layer, as the pictures were taken before the phenolphthalein indicator was sprayed, but are rather a consequence of the change in oxidation state of sulphur during BFS-OPC hydration. This oxidation process took place independent of carbonation, and created rings that were visible in all BFS:OPC pastes. Macrocracking is visible in Fig. 5 as radial lines. The structure is so open after carbonation that the oxidation of sulphur takes place through the cracks, giving further evidence to the effects of cracking.

Because of the extensive cracking that occurs during carbonation, the changes in permeability are significantly higher for both 9:1 BFS:OPC pastes as seen in Fig. 6. In fact, this cracking may have even

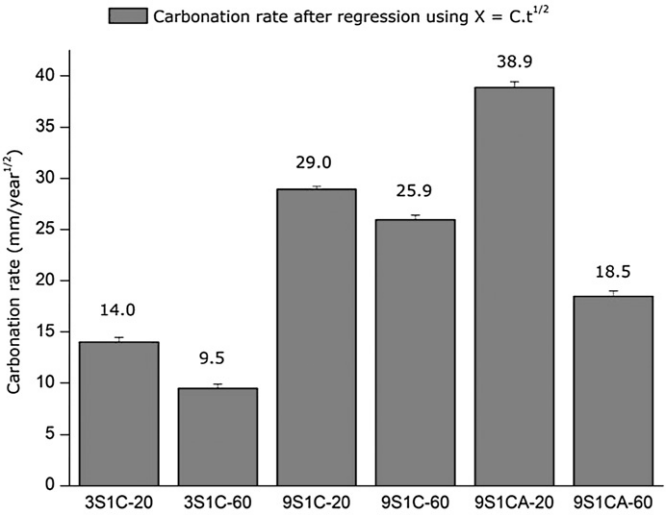

Fig. 2. Carbonation rate for BFS:OPC pastes studied.

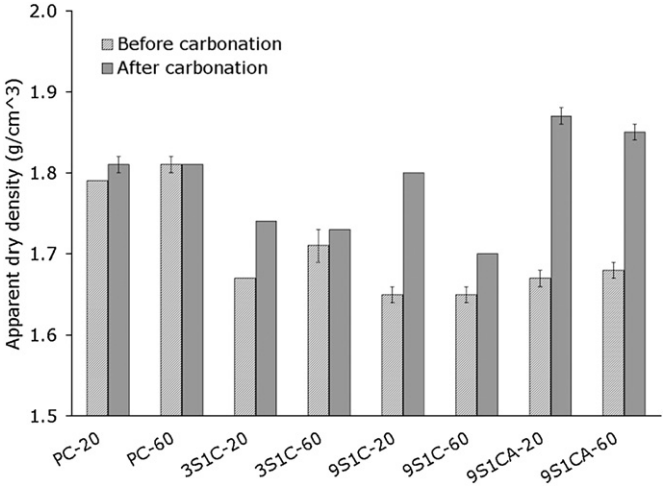

Fig. 3. Apparent dry density before and after carbonation for pastes studied.

increased when the samples were oven dried during preparation to oxygen permeability. The cracks were so large for 9S1CA, that gas permeability could not be measured for these pastes.

It is possible to see that PC pastes (neat OPC) did not have a significant change in permeability after carbonation, which confirms what has been said above regarding the carbonation of these pastes: calcium carbonate sealed the outer pores limiting further access of CO_2 to the inner structure. The changes in permeability after carbonation were higher for 9S1C than 3S1C pastes, i.e. with increasing amount of BFS in the pastes and especially with alkali activation. Permeability results have clearly shown that BFS:OPC pastes suffered carbonation shrinkage and cracking during testing, although carbonates have filled some pores, increasing the overall density and reducing overall porosity. It is questionable, therefore, whether apparent porosity (water density method) should be used to evaluate the changes in the structure after severe carbonation. Bier et al. [10] showed by mercury intrusion porosimetry (MIP), that in pastes containing high amounts of BFS the microstructure was coarsened. However, for the BFS:OPC pastes studied in this paper, MIP proved ineffective, as the samples were significantly soft after carbonation and the high vacuum pressure used in MIP equipment destroyed samples and gave inaccurate results.

3.4. Carbonation of CH and C–S–H

The cracking shown in Fig. 5 can be explained when carbonation of C–S–H is considered. Figs. 7–9 show the extent of carbonation of CH and C–S–H in pastes 3S1C, 9S1C and 9S1CA, respectively. These figures indicate that in all pastes, the amount of carbonates increased from 7 to 21 days, which justifies the increase in density previously discussed. In addition, curing at elevated temperature decreased the total amount of carbonates formed in all pastes at 7 and 21 days, except for the paste 9S1C where after 7 days carbonation, the total amount of carbonates increased slightly from 6.9% to 8.3%. Elevated temperature curing appears to promote the hydration of BFS and consequently reduce the carbonation attack, which also agrees with results in previous sections.

The C–S–H did not carbonate significantly in the 3S1C pastes, probably due to the higher amount of CH present before carbonation, i.e. 6.6% CH for 3S1C-20 and 7.2% CH for 3S1C-60 (Table 3). At 7 days,

Table 4
Change in apparent density (percentage) after 21 days of carbonation for the pastes studied.

PC-20	PC-60	3S1C-20	3S1C-60	9S1C-20	9S1C-60	9S1CA-20	9S1CA-60
0.7%	0.0%	4.2%	0.9%	8.1%	3.7%	10.8%	9.5%

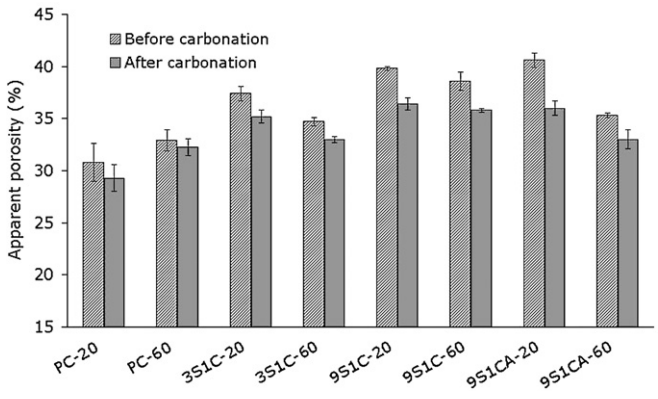

Fig. 4. Apparent porosity before and after carbonation for pastes studied.

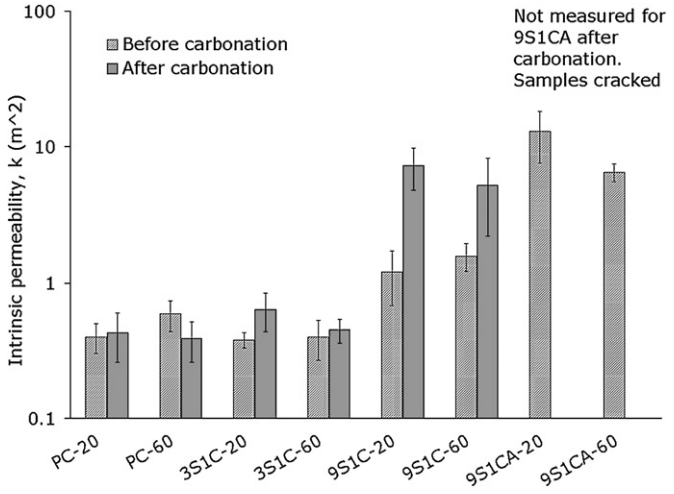

Fig. 6. Oxygen permeability (log scale) before and after carbonation for pastes studied.

only 0.3% and 0.1% of carbonates had formed from C–S–H for 3S1C-20 and 3S1C-60, respectively, while after 21 days of carbonation, only 1.7% had formed from C-S–H for both 3S1C pastes.

In the 9S1C and 9S1CA pastes, all of the CH had carbonated at 7 days. At 7 days 1.6% of the carbonates in 9S1C-20 had formed from C–S–H which increased to 6.1% at 21 days. For 9S1C-60, 3.1% of carbonates had formed from C–S–H at 7 days but only 5.4% at 21 days, less than in 9S1C-20. However, for 9S1CA pastes the carbonation was much more severe. In these samples the CH content before carbonation was only 0.9% and 0.6% for 9S1CA-20 and 9S1CA-60, respectively (Table 3). Most of the carbonates formed in these samples were from C–S–H. After 21 days, 12.3% of carbonates in 9S1CA-20 had formed from C–S–H out of a total carbonate of 13.5%. 9S1CA-20 not only carbonated more than its non-activated analogue 9S1C-20, but there was greater carbonation of C–S–H. In the 9S1CA-60 samples where CH levels were extremely low due to additional hydration, the total carbonation was lower, due to the lower overall porosity. The form of carbonation product in 9S1CA pastes is different and will be discussed below.

Figs. 10–12 show the DTG traces of the decarbonation region for pastes 3S1C, 9S1C and 9S1CA, respectively. In general, the decarbonation peaks shown by DTG were better defined after 21 days, as the extent of carbonation was higher. For 3S1C, the main peaks for decomposition of carbonates shifted to higher temperatures after 21 days and a shoulder at 730 °C–750 °C was present. This shoulder was present in all 9S1C pastes and its presence appears to be associated with the carbonation of C–S–H. The onset temperature of decarbonation started at 670 °C for pastes 3S1C after 21 days of carbonation and for all 9S1C pastes.

The decarbonation process in 9S1CA appeared to be different from the other two BFS/OPC pastes, as can be seen in Fig. 12. The decarbonation loss started much lower at approximately 550 °C and in the DTG curves was clearly divided in two steps, centred at about 620 °C and 700–720 °C, indicating that a different carbonate product, which decomposed at lower temperatures, has formed in 9S1CA pastes. According to Ghosh [30], aragonite is a calcium carbonate polymorph that dissociates earlier than calcite while Gaztanaga et al. [31] pointed out that the presence of other decarbonation maxima in the DTG of cement pastes is due to decomposition of either aragonite and vaterite or even amorphous carbonate. Thiery et al. [12] proposed three modes for the decomposition of calcium carbonate, all of them coexisting in the ultimate state of carbonation. Mode I (780 °C<T<990 °C) is supposedly associated with the decomposition of well-crystallized calcite. The presence of vaterite and aragonite causes the carbonates to decompose at lower temperatures, and defines Mode II (680 °C<T<780 °C). Finally, mode III (550 °C<T<680 °C) is probably associated with amorphous calcium carbonate.

Thus, it is possible that the changes in the DTG curve of 9S1CA are associated with the presence of either aragonite or amorphous carbonates in these pastes. Aragonite has been shown to undergo an endothermic transformation into calcite at approximately 400–420 °C [30,32]. Based only on the TGA and DTG evidence, it is not possible to confirm whether the lower onset temperature at 600 °C was due to decomposition of aragonite.

Figs. 13–15 show the XRD traces of the 3S1C, 9S1C and 9S1CA pastes, respectively, after 7 and 21 days of accelerated carbonation at 5% CO_2. The calcium carbonate polymorphs were identified as "V" for vaterite, "A" for aragonite and "CC" for calcite in the traces. Small

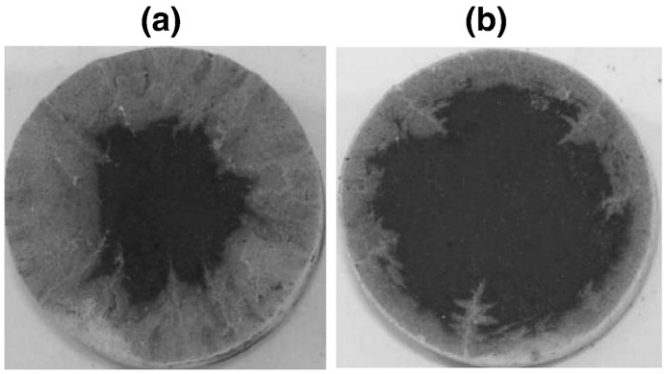

Fig. 5. Microcracking in (a) 9S1CA-20 and (b) 9S1CA-60 after 7 days of accelerated carbonation.

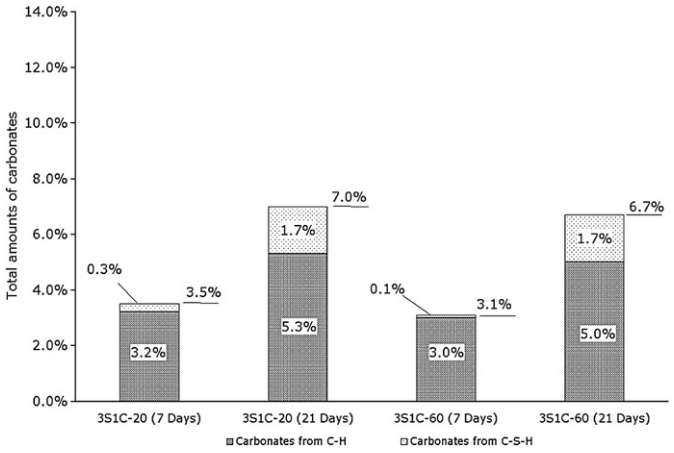

Fig. 7. Total amount of carbonates formed by carbonation of CH and C–S–H in 3S1C pastes after 7 and 21 days of accelerated carbonation.

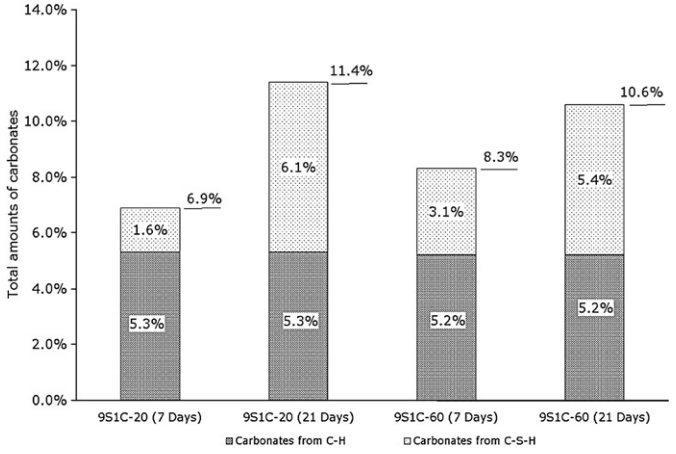

Fig. 8. Total amount of carbonates formed by carbonation of CH and C–S–H in 9S1C pastes after 7 and 21 days of accelerated carbonation.

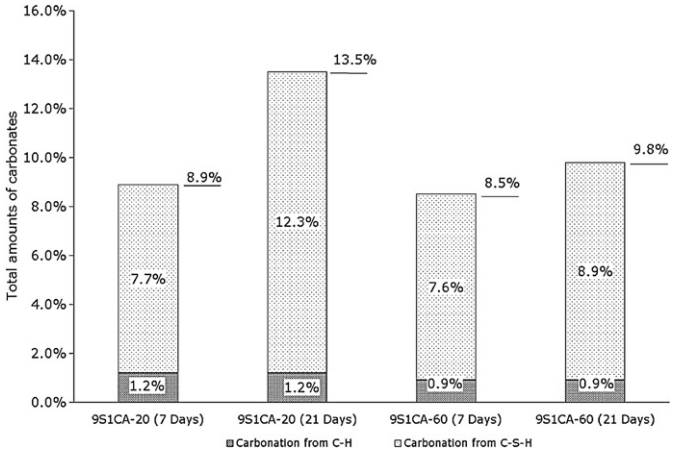

Fig. 9. Total amount of carbonates formed by carbonation of CH and C–S–H in 9S1CA pastes after 7 and 21 days of accelerated carbonation.

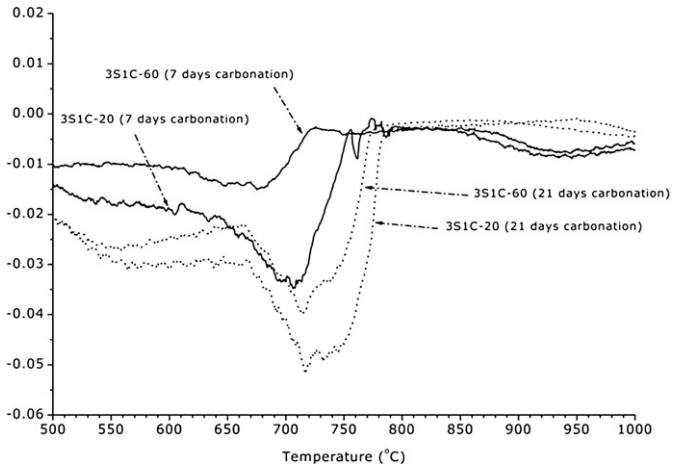

Fig. 10. Decarbonation region on DTG curve for pastes 3S1C after 7 and 21 days of accelerated carbonation.

peaks due to CH and gehlenite from unreacted BFS (G) were also identified. The small hump around $2\theta = 21°$ appears to be associated with the formation of poorly ordered silica (labeled as SiO_2), while the hump around $2\theta = 39°$ is due to poorly crystalline calcite and amorphous silica. So XRD shows that amorphous silica has been found for all BFS:OPC pastes after carbonation. Surprisingly, CH was still found

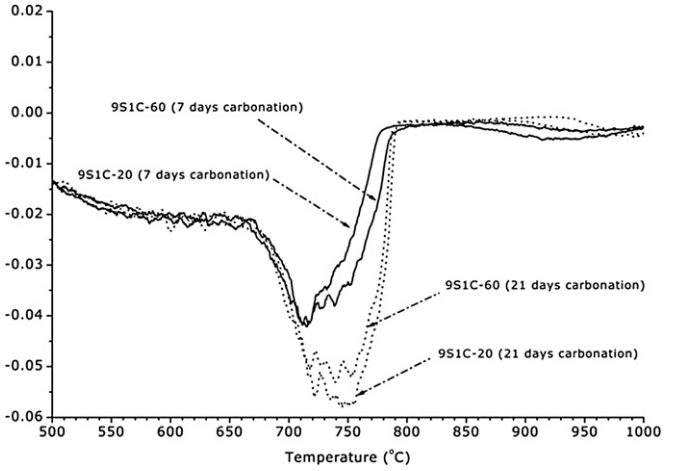

Fig. 11. Decarbonation region on DTG curve for pastes 9S1C after 7 and 21 days of accelerated carbonation.

in the carbonated zone of formulation 3S1C after accelerated carbonation. Traces of CH were also observed in 9S1C carbonated for 7 days but this had disappeared by 28 days. No CH was found in the 9S1CA pastes.

Vaterite and calcite were found as the main polymorphs of $CaCO_3$ in all pastes. The tests were performed in a carbonation chamber set at 25 ± 5 °C and 60% humidity, conditions under which both polymorphs can coexist [33]. XRD indicated that in a paste rich in CH before carbonation, i.e. 3S1C, CH remained even after 21 days of accelerated carbonation and only calcite and vaterite were formed as carbonated products.

Aragonite was only found by XRD in the 9S1CA samples. The presence of aragonite also coincided with a different DTG trace for the decomposition of carbonates in 9S1CA (Fig. 12). Black et al. [16] studied the carbonation of pure C–S–H (I) pastes in air and pointed out that vaterite forms preferentially on CH because of the similarities in their symmetries and their positive surface charge. In addition, the decalcification of C–S–H led to amorphous calcium carbonate until free silica was formed, whereupon the carbonate was converted into aragonite. In other words, it is the formation of silica gel that leads to the precipitation of aragonite as a carbonation product. This paste, 9S1CA, is the paste with lowest percentage of CH at 90 days, therefore, CO_2 will react with all calcium hydroxide rapidly, ultimately attacking the C–S–H forming more hydrous silica.

If the main concern for durability is the carbonation of C–S–H and cracking, our results suggest that using Na_2SiO_2 to activate 9:1 BFS: OPC formulations in order to improve the amount of hydration, leads

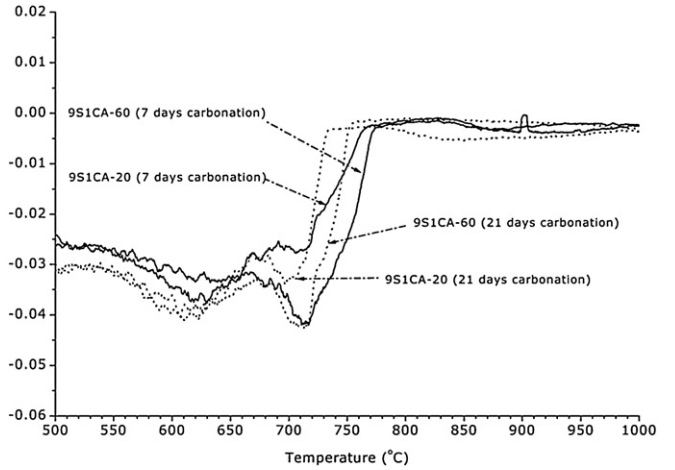

Fig. 12. Decarbonation region on DTG curve for pastes 9S1CA after 7 and 21 days of accelerated carbonation.

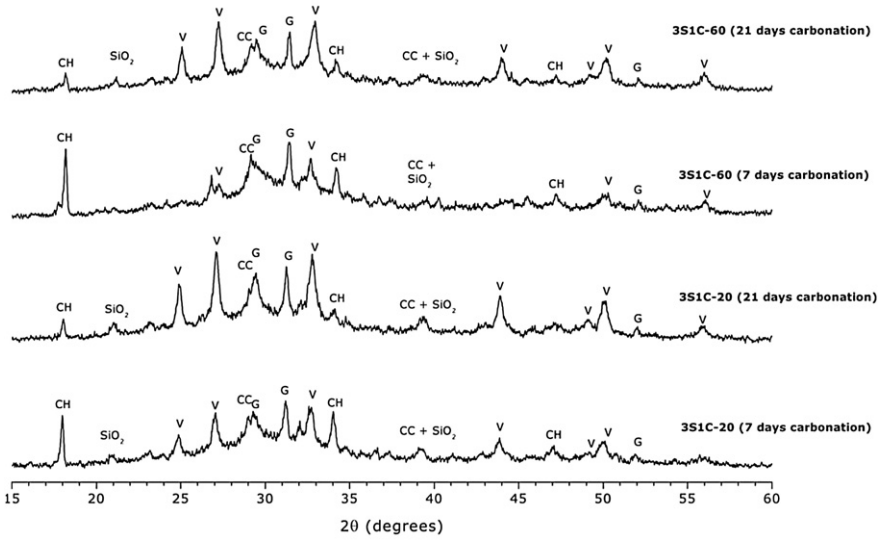

Fig. 13. XRD for 3S1C pastes after 7 and 21 days of accelerated carbonation.

to pastes that are less resistant to carbonation than the non-activated pastes and should be avoided.

The mechanism of carbonation in BFS/OPC pastes used for encapsulation seems to be governed mainly by the amount of CH available before carbonation starts, as previously suggested by Matala [27] for GGBS concretes. In pastes with a reasonable amount of CH (e.g. 6.6% in 3S1C-20 and 7.2% in 3S1C-60), the main carbonation products are calcite and vaterite from carbonation of CH. The decalcification of inner C–S–H takes place, but it is much slower because the calcium from CH enables longer buffering of the pore solution. Consequently, the transformation of the C–S–H structure takes longer. When only small amounts of CH are present (from 0.6% to 3.9% in 9S1CA and 9S1C), C–S–H is rapidly decalcified and the decalcification causes shrinkage with a significant rise in permeability.

4. Conclusions

BFS/OPC pastes used for encapsulation of nuclear wastes were cured at different temperatures (20 °C and 60 °C) and submitted to accelerated carbonation. This paper studied the effect of curing temperature on the carbonation rate, carbonation of the main phases (CH and C–S–H) and on the changes in apparent density, porosity and permeability after accelerated carbonation testing. The conclusions of this work are:

(a) Samples cured at elevated temperature, i.e. 60 °C, had lower carbonation rates and decreased levels of both total carbonation and C–S–H carbonation. This increased curing temperature promoted the hydration of BFS forming a denser microstructure, which reduced the diffusion of CO_2 into the matrices, improving the durability of these pastes to carbonation.

(b) Permeability results have clearly shown that all BFS:OPC pastes suffered carbonation shrinkage and cracking during testing, although carbonates have filled some pores, increasing the overall density and reducing overall porosity.

(c) The extent to which C–S–H was carbonated, increased as the initial amounts of CH present before carbonation decreased. In 3:1 BFS:OPC pastes there was still sufficient CH present to buffer the C–S–H carbonation. However, in both 9:1 BFS:OPC and the system activated with Na_2SiO_3, there were greater

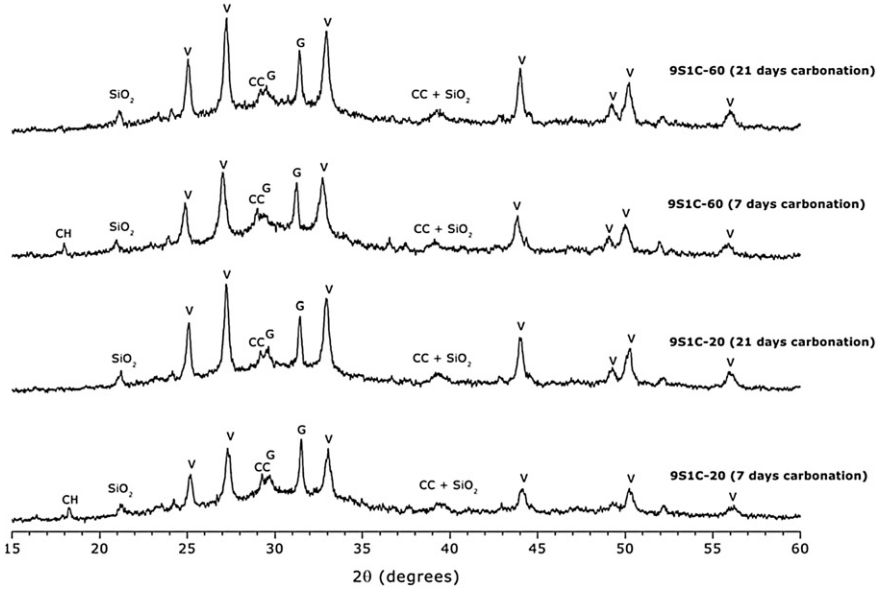

Fig. 14. XRD for 9S1C pastes after 7 and 21 days of accelerated carbonation.

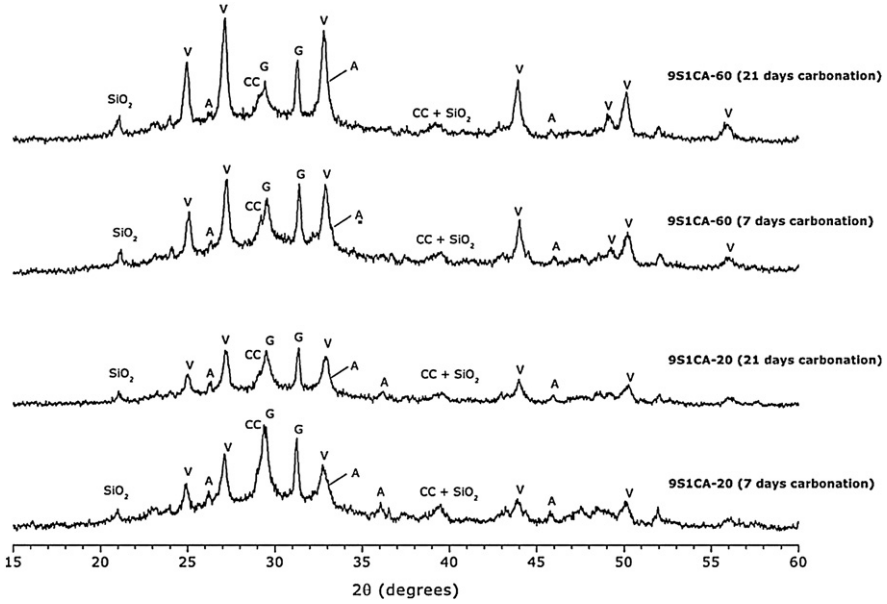

Fig. 15. XRD for 9S1CA pastes after 7 and 21 days of accelerated carbonation.

amounts of carbonated C–S–H. These systems might not be suitable for encapsulation if carbonation is a concern.

(d) The calcium carbonate phase formed appeared to be determined by the amount of available CH. Amorphous or poorly crystalline silica was found for all BFS:OPC pastes after carbonation. However, the presence of aragonite, together with a different decarbonation pattern in the DTG trace (i.e. decarbonation at lower temperatures) was associated with pastes with the lowest CH content prior to carbonation. Aragonite formation appeared to be a good indicator for C–S–H carbonation.

References

[1] C.R. Wilding, The performance of cement based systems, Cem. Concr. Res. 22 (1992) 299–310.
[2] J. Hill, J.H. Sharp, The mineralogy and microstructure of three composite cements with high replacement levels, Cem. Concr. Compos. 24 (2002) 191–199.
[3] C. A. Utton, "The encapsulation of a $BaCO_3$ waste in composite cements," PhD Thesis, The University of Sheffield, Sheffield, 2006.
[4] J.-P. Gorce, N.B. Milestone, Probing the microstructure and water phases in composite cement blends, Cem. Concr. Res. 37 (2007) 310–318.
[5] L.J. Parrott, A Review of Carbonation in Reinforced Concrete, Cement and Concrete Association, Wexham Springs, Great Britain, 1987.
[6] J.M. Chi, R. Huang, C.C. Yang, Effects of carbonation on mechanical properties and durability of concrete using accelerated testing method, J. Mar. Sci. Technol. 10 (1) (2002) 14–20.
[7] M.A. Sanjuan, C. Andrade, M. Cheyrezy, Concrete carbonation tests in natural and accelerated conditions, Adv. Cem. Res. 15 (4) (2003) 171–180.
[8] C. Gervais, A.C. Garrabrants, F. Sanchez, R. Barna, P. Oszkowicz, D. Kosson, The effects of carbonation and drying during intermittent leaching on the release of inorganic constituents from a cement-based matrix, Cem. Concr. Res. 34 (2004) 119–131.
[9] J.J. Chen, J.J. Thomas, H.M. Jennings, Decalcification shrinkage of cement paste, Cem. Concr. Res. 36 (2006) 801–809.
[10] T.A. Bier, J. Kropp, H.K. Hilsdorf, The formation of silica gel during carbonation of cementitious systems containing slag cements, Proc. 3rd CANMET/ACI Conf on the Use of Fly ash, Silica Fume, Slag and Natural Pozzolans in Concrete, Trondheim, Norway, Vol. 2, 1989, pp. 1413–1428, SP 114.
[11] G.W. Groves, A. Brough, I.G. Richardson, C.M. Dobson, Progressive changes in the structure of hardened C_3S cement pastes due to carbonation, J. Am. Ceram. Soc. 74 (11) (1991) 2891–2896.
[12] M. Thiery, G. Villain, P. Dangla, G. Platret, Investigation of the carbonation front shape on cementitious materials: effects of the chemical kinetics, Cem. Concr. Res. 37 (2007) 1047–1058.
[13] W.F. Cole, B. Kroone, Carbon dioxide in hydrated Portland cement, ACI J. 31 (1960) 1275–1295.
[14] P.A. Slegers, P.G. Rouxhet, Carbonation of the hydration products of tricalcium silicate, Cem. Concr. Res. 6 (1976) 381–388.
[15] Y. Lo, H.M. Lee, Curing effects on carbonation of concrete using a phenolphthalein indicator and Fourier-transform infrared spectroscopy, Build. Environ. 37 (2002) 507–514.
[16] L.C. Breen, J. Yarwood, K. Garbev, P. Stemmermann, Structural features of C–S–H (I) and its carbonation in air — a Raman spectroscopic study. Part II: carbonated phases, J. Am. Ceram. Soc. 90 (3) (2007) 908–917.
[17] T. Nishikawa, K. Suzuki, Chemical conversion of C–S–H in concrete, Cem. Concr. Res. 24 (1994) 176–182.
[18] L. Black, K. Garbev, I. Gee, Surface carbonation of synthetic C–S–H samples: a comparison between fresh and aged C–S–H using X-ray photoelectron spectroscopy, Cem. Concr. Res. 38 (6) (2008) 745–750.
[19] K. Suzuki, T. Nishikawa, S. Ito, Formation and carbonation of C–S–H in water, Cem. Concr. Res. 15 (1985) 213–224.
[20] J. Bensted, Raman spectral studies of carbonation phenomena, Cem. Con. Res. 7 (1977) 161–164.
[21] S. Martinez-Ramirez, S. Sanchez-Cortes, J.V. Garcia-Ramos, C. Doming, C. Fortes, M.T. Blanco-Varela, Micro-Raman spectroscopy applied to depth profiles of carbonates fromed in lime mortar, Cem. Concr. Res. 33 (2003) 2063–2068.
[22] M. Collepardi, S. Collepardi, J.J. Ogoumah Olagot, F. Simonelli, The influence of slag and fly ash on the carbonation of concrete, Proc. of the 8th CANMET/ACI Internat. Conf. on Fly Ash, Silica Fume, Slag and Natural Pozzolans in Concrete, Las Vegas, NV, U.S.A., SP-221, 2004, pp. 483–493.
[23] V.T. Ngala, C.L. Page, Effects of carbonation on pore structure and diffusional properties of hydrated cement pastes. Cem. Concr. Res. 27 (7) (1997) 995–1007.
[24] G.J. Osborne, Carbonation and permeability of blast furnace slag cement concretes from field structures, Proc. 3rd CANMET/ACI Internat. Conf. on the use of Fly Ash, Silica Fume, Slag and Natural Pozzolans in concrete, Trondheim, Norway, 1989, pp. 1209–1237, SP 114.
[25] J. Nakamoto, K. Togawa, A study of strength development and carbonation of concrete incorporating high volume blast furnace slag, 5th CANMET/ACI Internat. Conf. on the use of Fly Ash, Silica Fume, Slag and Natural Pozzolans in concrete, Milwaukee, 1995, pp. 1121–1139, SP 153.
[26] D.W.S. Ho, R.K. Lewis, Carbonation of concrete and its prediction, Cem. Concr. Res. 17 (1987) 489–504.
[27] S. Matala, Carbonation mechanism in the granulated blast furnace slag concrete, Proceeding of the 10th Internat. Cong. Chem. Cement, Gothenburg, Sweden, 1997, 4iv005.
[28] J.G. Cabrera, C.J. Lynsdale, A new gas permeameter for measuring the permeability of mortar and concrete, Mag. Concr. Res. 40 (144) (1988) 177–182.
[29] J.G. Cabrera, P.A. Claisse, Oxygen and water vapour transport in cement–silica fume pastes, Constr. Build. Mater. 13 (1999) 405–414.
[30] S.N. Ghosh, Advances in Cement Technology: Critical Reviews and Case Studies on Manufacturing, Quality Control, Optimization and Use, Pergamon Press, New York, 1981.
[31] M.T. Gaztanaga, S. Goni, A. Guerrero, M.S. Hernandez, Carbonation of hydrated calcium aluminate cement and ordinary Portland cements of varying alkali content, 10th Internat. Cong. Chem. Cem. Gothenburg, Sweden, 1997, 4v003.
[32] S. Goto, K. Suenaga, T. Kado, Calcium silicate carbonation products, J. Am. Ceram. Soc. 78 (11) (1995) 2867–2872.
[33] E.T. Stepkowka, J.L. Perez-Rodriguez, M.J. Sayagues, J.M. Martinez-Blanes, Calcite, vaterite and aragonite forming on cement hydration from liquid and gaseous phase, J. Therm. Anal. Calorim. 73 (2003) 247–269.